Polarimetric Signatures from Ice Crystals Observed at 95 GHz in Winter Clouds. Part I: Dependence on Crystal Form

MENGISTU WOLDE AND GABOR VALI

Department of Atmospheric Science, University of Wyoming, Laramie, Wyoming

(Manuscript received 6 August 1999, in final form 11 July 2000)

ABSTRACT

Based on observations made with an airborne 95-GHz polarimetric cloud radar and in situ microphysical probes, the dependence of Z_{DR} and linear depolarization ratio (LDR) values on ice crystal type and radar beam orientation was examined. Distinct ranges of Z_{DR} and LDR values at various radar beam orientations were identified for simple planar and columnar crystals and for melting particles. The results also show that, based on Z_{DR} and LDR values for different beam orientations, dendritic crystals can be distinguished from simpler hexagonal and branched crystals. Polarimetric signatures are almost exclusively associated with unrimed or slightly rimed crystals, therefore the presence of such signatures can help to identify cloud regions where such crystals dominate. The data generally agrees with previously reported results, though some differences are also noted. The observed Z_{DR} and LDR values for simple crystal types are in reasonable agreement with theoretical predictions.

1. Introduction

Variations in the shapes of ice crystals influence essentially all cloud processes, including precipitation development, radiative energy transfer, and cloud chemistry. Differences in crystal shapes arise from the dependence of crystal habit on temperature and supersaturation, and from the riming and aggregation of crystals. These complexities pose significant observational and modeling challenges. The importance of addressing these problems is underscored by the large fraction of clouds that are composed entirely or partially of ice particles both in the troposphere and in the stratosphere.

In situ data collected using instrumented aircraft or balloon sondes can provide detailed information about cloud composition, but such observations have limited spatial and temporal coverage. Observations by remote sensing provide much better sampling, but the utility of these measurements critically depends on the interpretation of the data in terms of fundamental quantities of interest. Microwave remote sensing, from the ground and from space, has been shown to be an effective tool for the characterization of clouds and of precipitation, and much effort is being invested in improving the understanding of these measurements. The recent extension of measurements to higher frequencies (>35 GHz; i.e., millimeter wavelengths) opened further opportunities and raised new questions. Approaches to enhance the utility of millimetric microwave measurements for cloud studies include combined uses of radars and lidars (e.g., Intrieri et al. 1993), radars and infrared radiometers (e.g., Matrosov et al. 1992), microwave radiometer and radar (e.g., Stankov et al. 1995; Politovich et al. 1995), and the use of multiple radar wavelengths (e.g., Sekelsky and McIntosh 1996).

While radar backscatter, expressed as reflectivity, is in itself quite useful for depicting cloud structure and as a measure of rain intensity, other radar parameters are needed to obtain more detailed information about cloud composition in terms of quantities relevant to the microphysics of clouds. Jameson and Johnson (1990) describe multiparameter radar methods used to retrieve raindrop sizes and to detect hailstones. Progress in the identification and characterization of ice clouds came from combining radar and radiometer measurements (Hakkarinen and Adler 1988; Matrosov et al. 1992; Intrieri et al. 1993; Matrosov 1997), from the combined use of radars and lidars (e.g., Intrieri et al. 1993), and from using two different radar wavelengths simultaneously (e.g., Sekelsky and McIntosh 1996; Sekelsky et al. 1999). The value of polarimetric measurements for the identification of hydrometeors was brought to attention by the early work of McCormick and Hendry (1975), Cox et al. (1978), Pasqualucci et al. (1983), Hall et al. (1984), and Aydin et al. (1984).

The fundamental basis for the utility of polarization in observing ice particles is the asymmetry of many ice

Corresponding author address: Dr. Mengistu Wolde, Institute for Aerospace Research, National Research Council of Canada, Ottawa, ON K1A 0R6, Canada.
E-mail: mengistu.wolde@nrc.ca

particle shapes. Of course, variabilities in size and shape, and the fact that oscillating motions alter the orientation of particles, introduce considerable complexities. Many of these factors are poorly observed and are difficult to treat theoretically. Even so, for simple crystal shapes, there is a considerable body of theoretical predictions of the polarimetric observables (Matrosov 1991a,b; Matrosov and Kropfli 1993; Vivekanandan et al. 1994; Matrosov et al. 1996; Reinking et al. 1997a; Aydin and Tang 1997; Aydin and Walsh 1999). Models have also been developed for melting crystals (Szyrmer and Zawadzki 1999; Fabry and Szyrmer 1999) but these models do not treat polarization aspects. The modeling study of Matrosov et al. (1996) showed that the identification of crystal type is facilitated by observing the variation of polarization parameters with the angle of incidence (elevation angle) of the radar beam with respect to the horizontal. Recent polarimetric observations have demonstrated the potential for identifying cloud regions containing ice particles, cloud droplets, or raindrops (Lohmeier et al. 1997; Reinking et al. 1997b), and in diagnosing ice crystal habit (Aydin et al. 1994; Vivekanandan et al. 1994; Pazmany et al. 1994b; Matrosov et al. 1996; Reinking et al. 1997a; Galloway et al. 1997).

In this paper, we present results obtained with an airborne 95-GHz (3-mm wavelength) radar. These results extend the existing body of polarimetric radar data and its interpretation. Specifically, (i) we analyze a larger dataset than those previously reported, (ii) our measurements also include data obtained at a horizontal radar beam orientation that is not practical with either ground-based or satellite-borne instruments, and (iii) we use simultaneous and coincident in situ measurements of ice crystal types and sizes for evaluating the radar observations. From these new measurements, we derive polarimetric signatures for selected ice crystal types, and in the accompanying paper (Part II; Wolde and Vali 2001) we present information on the frequency of occurrence of polarimetric signatures.

2. Instrumentation

The Wyoming King Air aircraft was used in this study together with the cloud radar installed in it. In addition to the measurements of thermodynamic state parameters and air motion, the in situ probes most relevant to this study are the 2D-C and 2D-P optical array probes (manufactured by Particle Measuring Systems Inc., Boulder, Colorado). The 2D-C probe has a resolution of 25 μm so that crystal shape is recognizable for sizes larger than about 150 μm. The 2D-P has a resolution of 200 μm and is most useful in this study for depicting large aggregates. The sampling rate of the 2D-C probe is about 5 L s^{-1}, while for the 2D-P probe it is about 40 L s^{-1}.

The Wyoming Cloud Radar (WCR) has a fixed antenna with a beamwidth of 0.7°. The radar beam can be set either in a side-looking mode (perpendicular to the flight path in a horizontal plane) or in an up-looking (vertical) direction. By making aircraft maneuvers at different roll angles, it is possible to attain a wide range of radar beam orientations. Under typical operating conditions, and for samples from the typical 120-m distance used in this study, independent radar records are obtained from cloud volumes of 260 m^3. The overall sampling rate, with the 1.5- or 3-km maximum range usually employed for the depiction of cloud structure, is much larger ($1.2–2.4 \times 10^6$ m^3 s^{-1}).

The WCR for these studies was set to transmit sequences of four pulses in single or dual polarization modes. In the single polarization mode the four pulses had horizontal polarization (HHHH). In the dual polarization mode each four-pulse sequence contained both H and V polarizations, typically in pairs (e.g., HHVV). In either mode, both the H and V components of the received signal are recorded. The orientation H and V have their actual meaning for the side-looking beam and can be considered as simply two orthogonal planes for the vertical pointing beam. Detailed information on the WCR is given by Pazmany et al. (1994a).

The WCR measurements are calibrated against a trihedral corner reflector for absolute values, and against natural distributed targets such as drizzle for determination of the cross-channel isolation. Postflight calibrations on the ground using the corner reflector were performed after every third or fourth flight. From these calibrations we conclude that the stability of the radar during the project was within 2 dBZ; the absolute accuracy of the reported values of the reflectivity factor is approximately ± 3 dBZ. With the assumption that drizzle produces negligible cross polarization for vertical beam orientation (< -34 dB according to Doviak and Zrnić 1993), the isolation between the H and V channels is limited by the leakage of copolarized signal into the cross-polar signal. This value was determined to be about -17 dB for the WCR, leading to a minimum detectable linear depolarization ratio of about -22 dB. Receiver noise level is recorded prior to the transmission of each pulse. Copolarized and cross-polarized signals presented in this paper were thresholded using this noise estimate, accepting only signals that exceeded the mean noise level by three standard deviations.

3. Polarimetric quantities

With the radar alternately emitting horizontally and vertically polarized power, four different values of the received power, and of the reflectivity factor Z, are possible: Z_{HH}, Z_{VV}, Z_{VH}, and Z_{HV}. By convention, the first index denotes the polarization of the received signal and the second index denotes the polarization of the transmitted power; values with equal indices are termed copolarized reflectivities, while values with two different indices are termed the cross-polarized reflectivities. From the four reflectivity values two quantities are commonly used to characterize the polarization behavior of

the scatterers: differential reflectivity (Z_{DR}) and linear depolarization ratio (LDR).

Differential reflectivity is the ratio of the radar backscatter cross sections in the two planes of polarization. It is defined (Seliga and Bringi 1976) as

$$Z_{DR} = 10 \log\left(\frac{Z_{HH}}{Z_{VV}}\right). \quad (1)$$

In general, Z_{DR} depends on radar beam orientation, particle aspect ratio, density (dielectric constant), and particle orientation (Bader et al. 1987). Beam orientation is here considered to depend only on the elevation angle with respect to the horizontal and will be termed the incidence angle, α. Since Z_{DR} is a ratio parameter, it is independent of particle concentration.

The LDR describes the relative magnitudes of the cross-polarized to the copolarized signals. It is defined as

$$\mathrm{LDR}_{HV} = 10 \log\left(\frac{Z_{HV}}{Z_{VV}}\right) \quad \text{and}$$

$$\mathrm{LDR}_{VH} = 10 \log\left(\frac{Z_{VH}}{Z_{HH}}\right). \quad (2)$$

For a reciprocal medium such as atmospheric hydrometeors, the cross-polarized components of the backscattered wave can be assumed to be equal, that is, $Z_{HV} = Z_{VH}$ (Doviak and Zrnić 1993; Aydin and Tang 1997). Combining (1) and (2) then leads to

$$\mathrm{LDR}_{HV} = \mathrm{LDR}_{VH} + Z_{DR}, \quad (3)$$

which we found to be always satisfied in our data within 1 dB. Because of this correspondence, only LDR_{HV} values are reported here and the subscript is dropped. One exception to this is in the data for needle crystals (Fig. 4; Table 1 lines 26, 27, and 34) where LDR_{VH} is reported since the radar on that occasion was operated in a single-polarization mode transmitting only H polarization. Based on the error analyses given by Pazmany et al. (1994a) and by Galloway et al. (1997), we estimate the accuracy of our Z_{DR} and LDR measurements as 0.5 and 2 dB, respectively.

Spurious Z_{DR} and LDR measurements can result from propagation effects. Owing to the shapes and typical fall patterns of atmospheric hydrometeors, the attenuation by hydrometeors is higher for the H polarized signal than for the V polarized signal for $\alpha \approx 0°$. This differential attenuation tends to reduce Z_{DR} values, increase LDR_{VH}, and decrease LDR_{HV} (Herzegh and Jameson 1992; Bringi et al. 1996). Such errors are small in our data because of the low reflectivities encountered and because of the close range of the observations. Exceptions are the melting layer and graupel cases.

4. Theory

In general, both Z_{DR} and LDR depend on the asymmetry of shapes of the scatterers and on the orientation of the symmetry axes relative to the direction of the incident beam. If the major axis of some strongly asymmetric scatterer coincides with the plane of polarization of the incident beam then high values of Z_{DR} will result. If the axes of this same scatterer lie at some angle to the plane of polarization of the incident beam, then high values of LDR will be produced and the value of Z_{DR} will be reduced.

For clouds consisting of ice crystals, the governing factors are expressed as the size-dependent aspect ratios (ratio of major to minor dimensions) of the crystals, their densities[1] (which determine their refractive indices), and their orientations (range of canting angles for free-falling oscillating crystals). Thus, for a horizontally directed and horizontally polarized incident wave, pristine crystals of relatively high densities, large aspect ratios, and near-horizontal major axes will produce a strong copolarized backscattered signal (with intensity depending on the number and size of crystals), and a considerably weaker cross-polarized component, that is, small values of LDR. For a vertically polarized but still horizontally directed incident wave, the same crystals will have a small reflectivity, so that Z_{DR} will be large. However, if these same crystals also exhibit a significant range of orientations (canting angles), perhaps as a result of complicated fall patterns, higher LDR and lower Z_{DR} will be observed. With a vertically directed beam, $\alpha \approx 90°$, the random orientation of crystals with respect to the vertical direction [except perhaps in strong electric fields, such as described by Galloway et al. (1997)] is expected to yield copolarized reflectivities independent of the plane of polarization, and hence $Z_{DR} \approx 0$ dB. On the other hand, crystals with strong asymmetry in their horizontal projection, like needle crystals falling with their long dimension nearly horizontally, are expected to produce the highest values of LDR for vertical beam incidence. Near-spherical shapes, like aggregates of low density, graupel, and hail can be expected to yield neither Z_{DR} nor LDR values of interest at any incidence angle due to their near-isometric shapes.

Since cross-polar signals, and the polarization dependence of the copolarized signals, is linked to the asymmetry of the scatterers, and since riming tends to diminish crystal asymmetry, polarization data provide, at a minimum, an indication of the relative prevalence of pristine crystals versus graupel. This is the primary motivation for examining the frequencies of significant polarimetric signatures in Part II.

With water-coated ice crystals in a melting layer, and possibly during riming in mixed phase cloud volumes, the effects of shape and canting on LDR are magnified

[1] Density is defined here as the ratio of actual volume to the volume of an enveloping cylinder; in some sources this is referred to as ''bulk density.'' At this time, neither in the modeling of microwave scattering by crystals, nor in the observations can the influence of included air pockets be treated.

TABLE 1. Summary of polarimetric observations for different crystal types.

	Date (M/D/Y)	Time (UTC)	α (°)	T (°C)	Type	Size (μm)	Z_{eHH} (dBZ)	Z_{DR} Mean	Z_{DR} 90%	Z_{DR} Max	LDR_{HV} Mean	LDR_{HV} 90%	LDR_{HV} Max
Part (a): Observations at near-horizontal radar beam angles, $\alpha < 25°$.													
1	02/18/97	1606:50–1606:55	2	−15.5	P1a	250–600	−7	4.6	5.3	5.8	−18.2	−15.7	−14.4
2	02/18/97	1552:10–1552:13	3	−13.2	P1a	600–1500	−6	6.4	7.1	7.6	−16.2	−13.9	−12.1
3	02/18/97	1553:26–1553:34	1	−13.7	P1d	500–1300	−10	7.0	7.7	8.6	−15.3	−12.4	−10.6
4	02/18/97	1607:48–1607:52	8	−15.6	P1a/P1d	500–1300	−3	6.4	7.1	7.4	−17.8	−14.9	−11.7
5	02/18/97	1619:49–1619:58	1	−13.3	P1a/P1d	600–1500	−4	6.2	7.2	8.0	−16.0	−13.7	−11.1
6	04/02/97	2025:15–2025:30	2	−6.2	R4a	800–1600	5	0.7	1.2	2.0	<−22	−20.4	−17.5
7	03/28/97	0017:00–0017:05	1	−13.2	R4a	800–1500	4	0.8	1.1	1.4	<−22	−19.1	−16.3
8	04/02/97	1829:35–1830:45	1	−11.5	P1e	3000–6000	−14	2.3	2.9	3.8	−14.2	−12.6	−10.5
9	04/02/97	1836:36–1837:00	1	−13.8	R2b	2600–4400	−5	0.7	1.3	1.8	−17.0	−15.0	−12.8
10	09/06/95	1733:48–1733:58	1	−5.6	R1a/few R2b	2100–5000	2	2.2	2.7	3.8	−19.8	−17.1	−15.7
11	09/06/95	1737:50–1737:58	25	−5.5	R1a/few R2b	1000–3000	−10	2.2	2.8	3.6	ND	ND	ND
12	02/18/97	1620:47–1620:57	6	−13.8	P1d/R2b	1000–4000	3	2.3	3.0	5.1	−18.2	−15.8	−12.5
13	03/24/97	1744:40–1744:50	0	−13.5	P1a/P1d/R3b	500–1500	−3	2.1	2.8	3.5	−17.4	−15.1	−12.0
14	02/18/97	1620:18–1620:24	4	−13.6	P1a/R3b	2000–3000	3	3.0	3.6	4.1	−17.7	−15.4	−14.4
15	03/13/97	0005:40–0006:22	0	−14.6	P1e/R2b	2000–4000	4	1.5	1.9	2.7	−15.8	−14.0	−11.6
16	02/11/97	2253:40–2254:00	1	−12.7	P1a/CP1a	400–800	3	1.6	2.0	2.5	<−22	−19.4	−16.5
17	02/11/97	2307:30–2307:55	2	−12.5	P1a/CP1a/R4b	400–1000	8	1.2	1.6	2.2	−19.8	−16.9	−13.4
18	09/06/95	1645:20–1645:30	25	0.8	ML	700–1300	1	2.2	2.7	3.3	−18.1	−14.6	−12.4
19	09/06/95	1645:50–1646:50	25	—	ML	—	15	1.2	1.8	2.8	−13.3	−11.2	−9.1
20	03/23/97	0013:20–0014:00	3	−14.3	R4b/R4c	3000-6000	13	0.9	1.5	2.6	−12.7	−9.3	−6.4
21	04/04/97	2100:50–2101:10	3	−6.5	R4b/R4c	3000–6000	19	−0.5	0.4	1.5	−9.7	−7.4	−5.7
Part (b): Observations at near-vertical radar beam angles, $\alpha > 65°$.													
22	02/18/97	1542:10–1542:30	87	−12.7	P1a	600–1000	−22	0.0	0.4	0.9	ND	ND	ND
23	02/18/97	1558:23–1558:42	88	−13.6	P1d	500–1000	−24	0.0	0.7	1.0	ND	ND	ND
24	02/18/97	1544:18–1544:35	89	−13.4	P1a/P1d	500–1500	−8	−0.1	0.3	1.1	<−22	−20.2	−17.4
25	04/02/97	1828:30–1829:30	89	−12.0	P1e	3000–6000	−3	0.2	0.5	1.0	<−22	−19.7	−15.5
26*	09/06/95	1715:05–1715:10	86	−0.5	R1a	600–1500	−9	—	—	—	−19.3	−16.4	−14.1
27*	09/06/95	1726:10–1726:14	87	−5.5	N1a	—	7	—	—	—	−18.7	−16.5	−14.3
28	03/02/97	2134:10–2134:20	88	−40.0	C1c/C2a	300–800	−14	0.3	0.6	1.3	−19.4	−17.2	−14.5
29	02/11/97	2221:39–2222:28	74	−28.8	C1c/C1e	300–600	−18	0.1	0.5	1.3	−19.0	−16.3	−12.3
30	02/11/97	2224:10–2224:40	85	−28.0	C2a	400–800	2	0.1	0.5	1.1	−22	−19.1	−16.2
31	02/11/97	2305:20–2305:35	89	−12.2	P1a/Cp1a	500–1200	6	0.0	0.3	0.8	<−22	−19.4	−17.0
32	02/11/97	2308:00–2308:10	84	−11.6	P1a/Cp1a/R4a	500–1200	8	0.0	0.4	0.8	<−22	−19.2	−16.6
33	09/06/95	1658:50–1659:05	87	—	ML	—	15	−0.1	0.3	0.9	−14.0	−11.4	−9.6
34*	09/06/95	1721:05–1721:10	89	—	ML	—	16	—	—	—	−11.6	−9.7	−7.9
35	03/23/97	0010:45–0011:05	88	−14.5	R4b/R4c	3000–6000	14	0.1	0.8	1.9	−16.3	−14.4	−12.2
36	04/04/97	2048:00–2048:15	73	—	R4b/R4c	—	19	−0.1	0.8	2.3	−13.4	−11.3	−8.8

— indicates no data.
ML indicates melting crystal in the melting layer.
ND indicates ''not detectable.''
* indicates LDR values in these lines are $LDR_{VH.}$

due to the high dielectric constant of water. This property of the radar bright bands was reported by Lohmeier et al. (1997) and Galloway et al. (1997) for millimeter wavelengths.

Quantitative evaluations for millimeter wavelengths of the trends described above have been given by various authors. Evans and Vivekanandan (1990) used a ''discrete dipole approximation'' to calculate the scattering properties of crystals, assumed a power-law size distribution, and assumed the major axes of the crystals to be in horizontal. Matrosov (1991a) and Reinking et al. (1997a) approximated crystals as prolate and oblate spheroids and calculated scattering properties by the Rayleigh approach, assigned a typical size, but allowed axis orientations to vary according to Gaussian functions. Aydin and Tang (1997, hereafter AT97) and Aydin and Walsh (1999, hereafter AW99) employed the ''finite difference time domain'' method, simulating complex crystal shapes with size distributions defined by gamma functions and with orientations assumed to follow Gaussian distributions. Common to all of these calculations is the use of expressions of the form $l = ad^b$ for the relationship between length (l) and diameter (d), with the constants a and b taken from observations.

In comparing observations with the model results, it is clear that there is a significant gap between the detail generally available from the observations and the large number of assumptions involved in the calculations. This is a serious limitation since the magnitudes of the computed quantities are as strongly influenced by the sizes, aspect ratios, and oscillation angles of the crystals as by their growth habits. However, the calculations indicate that recognition of crystal types from radar polarimetric data is possible through the combined use of Z_{DR} and LDR, and through the dependence of these quantities on incidence angle.

5. Results

Data were collected in flights made around Wyoming and Colorado during the period February to April 1997. A total of 52 h of data were obtained from cumulus, altocumulus, nimbostratus, and cirrus, covering the temperature range $-45°$ to $+6°$C. Additional data were used from one flight in nimbostratus over Oregon in September 1995.

For purposes of this study, data segments were selected for which crystal types were unchanged, as judged by eye from the images recorded by the 2D probes. For unrimed crystals of several hundred micrometer sizes the designation of crystal type is fairly unambiguous. For smaller sizes and for rimed crystals, there is a greater degree of uncertainty in type designation. Cloud regions of a few hundred meters in extent were usually sufficient to provide stable averages of the radar parameters. Even so, cloud regions as large as possible were used, consistent with homogeneity, in order to minimize the effects of local variabilities on the scale of the distance between the radar sample volume and the in situ probes. Radar data were used from the minimum usable radar range gate of 90 m to a maximum of 150 m. The latter restriction was relaxed for data from melting bands, but no crystal type is specified for those cases.

Observations for different crystal types[2] are listed in Table 1 for the two most frequently used ranges of radar incidence angles ($\alpha \leq 25°$ and $\alpha > 70°$). Data segments with one given crystal type are listed first, then those cases where mixtures of different crystal types occurred. In the latter cases, crystal types are listed with the dominant type first, followed by those appearing in smaller numbers during the data segment. For each observation, the mean, the 90th percentile, and the maximum values of Z_{DR} and LDR are listed. The column labeled Z_{eHH} gives the mean value of the measured reflectivity for horizontal polarization. The sizes of the crystals were determined from the 2D images. The size ranges indicated are those that contributed 90% of the radar reflectivity, computed using results from AW99 with an assumed mean canting angle (θ) of 0° and standard deviation of canting angle (σ_θ) of 5°. For Ple crystals the equations for P1d crystals were used with an extrapolation to 6-mm crystal sizes.

In the following sections we discuss observations for specific crystal types in terms of the dependence of Z_{DR} and of LDR on radar incidence angle, including observations at all available angles not just those presented in Table 1. The main results are given in Figs. 1–6. In these diagrams, mean values and standard deviations are indicated; data are shown only for α intervals for which at least 20 data points were available. The number of observations included in these figures range from six hundred to about ten thousand.

a. Planar crystals

1) UNRIMED HEXAGONAL PLATES (P1a) AND STELLAR (P1d) CRYSTALS

These two crystal types show similar polarimetric signatures so they are combined in this analysis. Typically these crystal types were observed in relatively shallow altocumulus with tops near $-16°$C. Figure 1 summarizes the data obtained for these crystal types and examples of the corresponding 2D images are also given. Lines 1–5 and 22–24 of Table 1 also refer to these data.

The Z_{DR} values observed with these crystals are higher than for any other crystal type. The observed value

[2] The designation of crystal types follows Magono and Lee (1966). Basic types used in this paper are: P1a—hexagonal plates; P1d—branched or stellar; P1e—dendritic; C1c—solid bullet; C1e—solid column; C2a—bullet rosett; CP1a—capped column; N1a—needle; R1a—rimed needle; R2b—densely rimed stellar; R4a—hexagonal graupel; R4b—lump graupel; R4c—conical graupel.

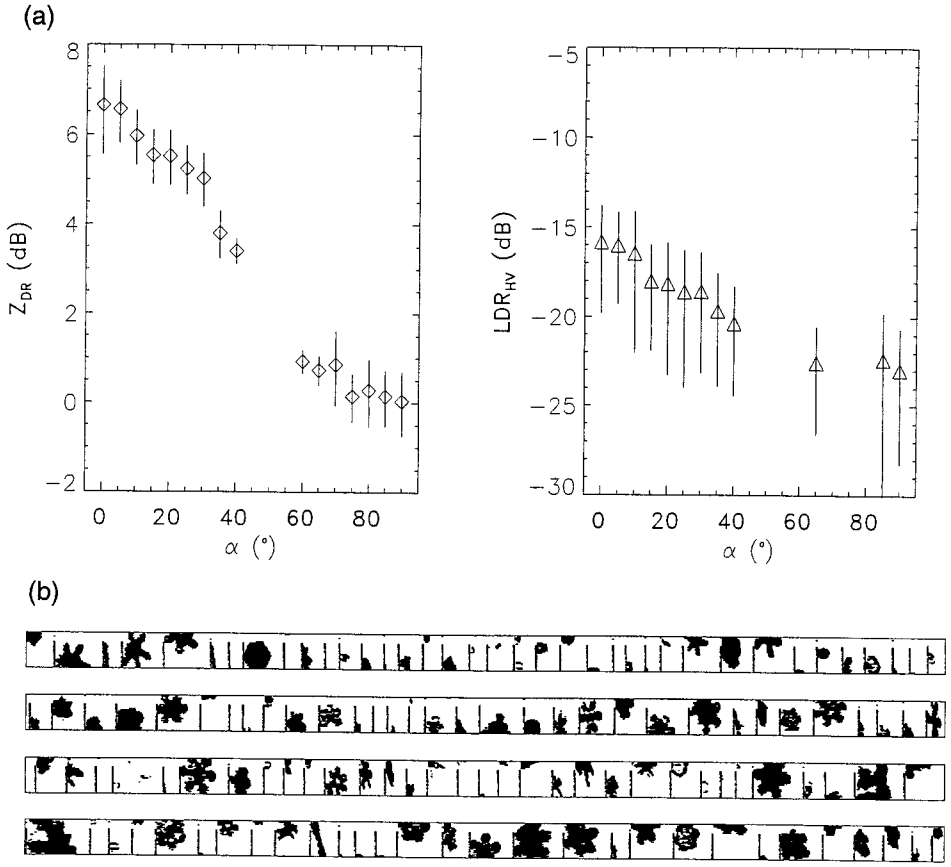

FIG. 1. (a) Variation of Z_{DR} and LDR_{HV} with radar beam incidence angle, α, in cloud regions of hexagonal plate (P1a) and/or stellar (P1d) crystals listed in lines 1–5 and 22–24 of Table 1. Means and standard deviations are indicated. Number of data points per α interval varies between a minimum of 20 and many thousands, depending on the flight pattern during data collection. (b) Sample 2D-C images of the types of crystals included in this graph. The widths of the image strips is 800 μm.

of $Z_{DR} = 7$ dB at $\alpha = 0°$ matches the calculations of AT97 in which an assumed size distribution is used and σ_θ is assumed to be 17°. However, using the observed size distributions of crystals, the size-dependent scattering cross sections given by AW99 for $\sigma_\theta = 5°$, the predicted Z_{DR} values are 2–3 dB higher than measured. Thus, it seems likely that canting angles in the clouds we sampled were, in fact, in the range 10°–20°. The Z_{DR} decreases with increasing α, as shown in Fig 1. The Z_{DR} decreases most rapidly in the interval $\alpha = 20°$–$60°$, becoming asymptotic near $\alpha = 90°$; this pattern matches the predictions of AT97 fairly well.

The maximum observed LDR value, for horizontal incidence, is −16 dB, which is considerably lower than the computed −8 to −11 dB given by AT97 for $\sigma_\theta = 10°$–$30°$. Values of −13 to −15 dB were obtained for the actual size distributions using the parametric fits of AW99 for $\sigma_\theta = 5°$. LDR also decreases with increasing incidence angle for these planar crystals. The observed decrease of about 6 dB by 45° is less than the calculated 10 dB decrease for the canting angles indicated by the Z_{DR}.

The discrepancy that emerges in LDR values, if the canting angles are derived from the Z_{DR} values, may be an indication that the aspect ratios of the crystals in our data were smaller than those assumed in the model calculations. With smaller aspect ratios, the canting angles also have to be assumed to be less than the 10°–20° deduced above.

Both Z_{DR} and LDR increase with increasing crystal sizes of P1a/P1d types (e.g., line 1 vs lines 2–3 of Table 1). This size dependence is consistent with an increase in aspect ratio for increasing sizes.

2) RIMED PLATE AND BRANCHED CRYSTALS (R4a)

The Z_{DR} and LDR_{HV} values for heavily rimed, but still recognizably hexagonal, P1a and P1d crystals are listed in lines 6–7 of Table 1. At horizontal incidence, Z_{DR} for these particles ranges from 0 to 2 dB, and LDR values are below the detection limit (~−22 dB). The decrease in the magnitudes of the polarimetric signatures in comparison with the smaller pristine plate and stellar crystals is a result of the decrease in aspect ratio and the decrease

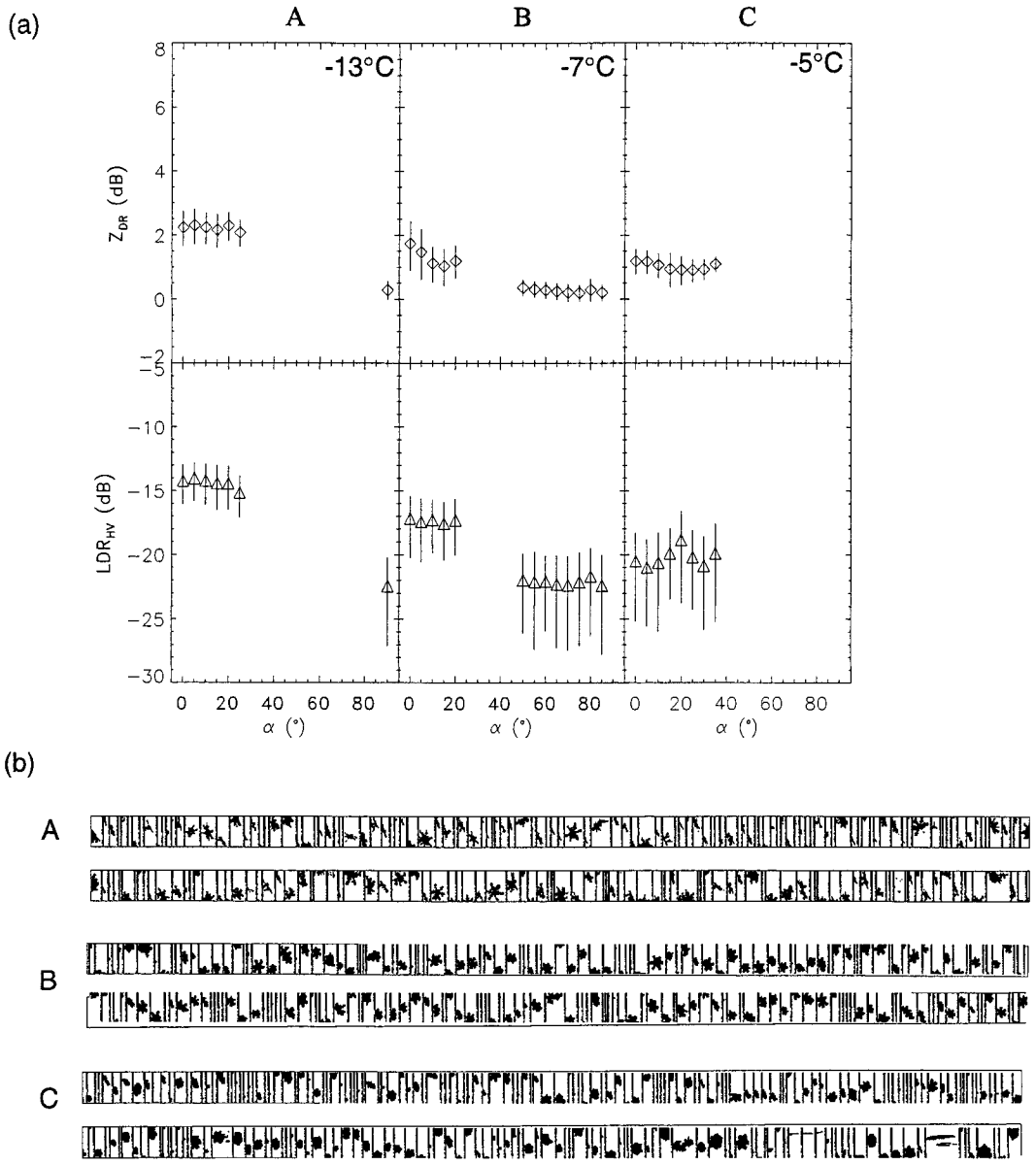

FIG. 2. (a) Same as Fig. 1 except for dendrite crystals listed in lines 8, 9, and 25 of Table 1: A—lightly rimed, P1e; B—moderately rimed, R1d; and C—densely rimed crystals, R2d. (b) Samples of 2D-P images. The width of each strip represents 6.4 mm.

in the bulk density. At the same time, the larger mass and scattering cross sections of these crystals is evident in the larger Z_e values.

3) DENDRITIC CRYSTALS (P1e, R1d, R2b)

Observations in a nimbostratus (2 April 1997) provided an opportunity to document the polarization characteristics of dendritic crystals with various degrees of riming. Samples were obtained during a descent in the cloud. Crystals were generally 2–4 mm in size with concentrations of up to 2 L^{-1}; the reflectivity factor Z_{eHH} increased from near −20 to 0 dBZ as the degree of riming increased. Some of these data are included in lines 8, 9, and 25 of Table 1.

To demonstrate the effect of riming on Z_{DR} and LDR the data are divided into three segments: A—unrimed to lightly rimed; B—moderately rimed; and C—densely rimed and turning into graupel. The Z_{DR} and LDR_{HV} trends with α, and samples of 2D-P images for these segments are shown in Fig. 2.

The data for segment A were taken a few hundred meters below cloud top between 1828:27 and 1830:45 UTC. The temperature was -13 ± 1°C, and crystals were mainly P1e with little or no sign of riming. For near-vertical beam ($\alpha \geq 85°$), Z_{DR} is 0 ± 0.5 dB, and

LDR_{HV} is below the -22 dB detection limit. At low radar incident angles ($\alpha \leq 25°$), the mean Z_{DR} is 2 ± 0.5 dB and LDR_{HV} is -15 ± 2 dB, with apparently weak dependence on α. Having low Z_{DR} values and high LDR values for horizontal incidence with the unrimed P1e crystals suggests high degree of canting of these crystals. However, the high LDR is unexpected for the low bulk density (0.4–0.5 g cm^{-3}) expected for these 2–4-mm-sized P1e crystals, as low density tends to reduce the polarimetric signatures (Reinking et al. 1997a). These polarimetric signatures for unrimed P1e crystals (low Z_{DR} and high LDR) were found frequently in our data.

The data for segment B were taken near midcloud level between 1834:50 and 1837:50 UTC. The temperature was -7 ± 3°C and crystals were the lightly to moderately rimed R1d type. The mean Z_{DR} decreases from 1.8 ± 0.5 dB at $\alpha < 5°$ to close to 0 dB for $\alpha \geq 60°$, while the mean LDR_{HV} decreases from -17 ± 2 dB for $\alpha < 25°$ to < -22 dB for $\alpha \geq 60°$. Comparing these values with those observed in segment A show the effects of riming in reducing both Z_{DR} and LDR_{HV} signatures for low elevation angles; Z_{DR} and LDR_{VH} were lower by about 0.5 and 2 dB, respectively, when compared with the values observed in segment A. These decreases both in Z_{DR} and LDR values could be a result of a decrease in the crystal aspect ratio, and/or a change in bulk density as a result of riming.

Segment C represents observations near cloud base (1838:10 to 1838:40 UTC) in densely rimed R2b crystals, which were turning into graupel. Temperature was -5 ± 2°C. At low α, Z_{DR} is 1 ± 0.25 dB and LDR_{HV} is < -22 dB, that is, a significant decrease in polarimetric signatures, particularly for LDR_{HV}, when compared with values obtained in segments A and B.

b. Columnar crystals

1) NEEDLE CRYSTALS (N1a, R1a)

Columnar crystal types N1a and R1a were observed on 6 September 1995 near the Oregon coast in a nimbostratus. The temperature at the locations of these crystals was -6 ± 2°C. The ice crystals were mainly of 300–1000-μm sizes with concentrations up to 65 L^{-1}. A few large (4–6 mm) densely rimed crystals were also present, particularly during the flight segments when data were being collected with a horizontal beam.

During most of the flight time, the radar was set to transmit H polarization only, as a result, few observations of Z_{DR} are available, and only LDR_{VH} data were collected. Data for these crystals are listed in lines 10–11 and 26–27 of Table 1. Figure 3 shows plots of Z_{DR} and LDR_{VH} versus α, and samples of 2D-C images. For the two α values, $Z_{DR} \approx 2 \pm 0.5$ dB. The LDR_{VH}, on the other hand, increases from about -22 dB at $\alpha \approx 0°$ to -18 ± 1 dB for $\alpha > 80°$. These Z_{DR} and LDR_{VH} observations have some differences and similarities with the AT97 result. The Z_{DR} values are comparable to the AT97 results for $\sigma_\theta = 30°$, while the LDR_{VH} values are comparable to the AT97 result for $\sigma_\theta = 5°$. Since the lower than expected Z_{DR} does not occur together with high LDR, it is likely that the presence of the large rimed crystals in the radar volumes reduced the values of both variables. The LDR values for near-vertical incidence angles are also lower than the AT97 results by about 4 dB.

2) COMBINATIONS OF COLUMNAR CRYSTALS

On a number of flights during the WYICE97, combinations of columnar crystals (bullets and columns) with size <1000 μm were observed in cirrus clouds at temperatures of $-25°$ to -40°C. Summaries of these observations for near-vertical beam are listed in lines 28–30 of Table 1. Insufficient data were collected to study the trends of the polarimetric signatures with α. The data at near-vertical beam had characteristics similar to those of needles. The high LDR values (> -19 dB) for near vertical beam are similar to the polarimetric signatures of needle crystals.

c. Mixtures of different crystal types

Since P1a and P1d crystals have similar polarimetric signatures (compare lines 2 and 3 in Table 1), their mixtures show similar signatures (Table 1, lines 4 and 5). In contrast, polarimetric signatures from slightly to moderately rimed, large (>1 mm) dendritic crystals (P1e, R1d, R2b) mixed with smaller (500–1000 μm) P1a and P1d types are closer to the polarimetric signatures of dendritic types (Table 1, line 12 vs line 9). In general, Z_{DR} and LDR values of smaller crystals are suppressed if they are mixed with other crystals having low polarimetric signatures but large contributions to the total radar return. For example, mixtures of P1a with capped columns (CP1a) produced weaker Z_{DR} and LDR values than P1a crystals by themselves (Table 1, lines 16–17 vs lines 1–2).

d. Melting layer (ML) observations

Polarimetric signatures from melting crystals are well documented for longer wavelengths; here we present a single case, from 6 September 1995, as a comparison. The melting crystals were columns, dendrites, and aggregates of various sizes (0.5 to >6 mm).

Data from ML are listed in lines 18–19 and 33–34 of Table 1. The Z_{DR} and LDR versus α from three radar bins ($\approx$90 m) at the center of the melting layer are shown in Fig. 4, along with sample 2D-C images. As with other crystals, Z_{DR} decreases from near 2 ± 0.5 dB at $\alpha \approx 15°$ to 0 ± 0.5 dB at $\alpha > 60°$. These Z_{DR} values for low α are comparable to values reported in the literature and consistent with the nonspherical shape of the melting crystals. In contrast, LDR is maximum

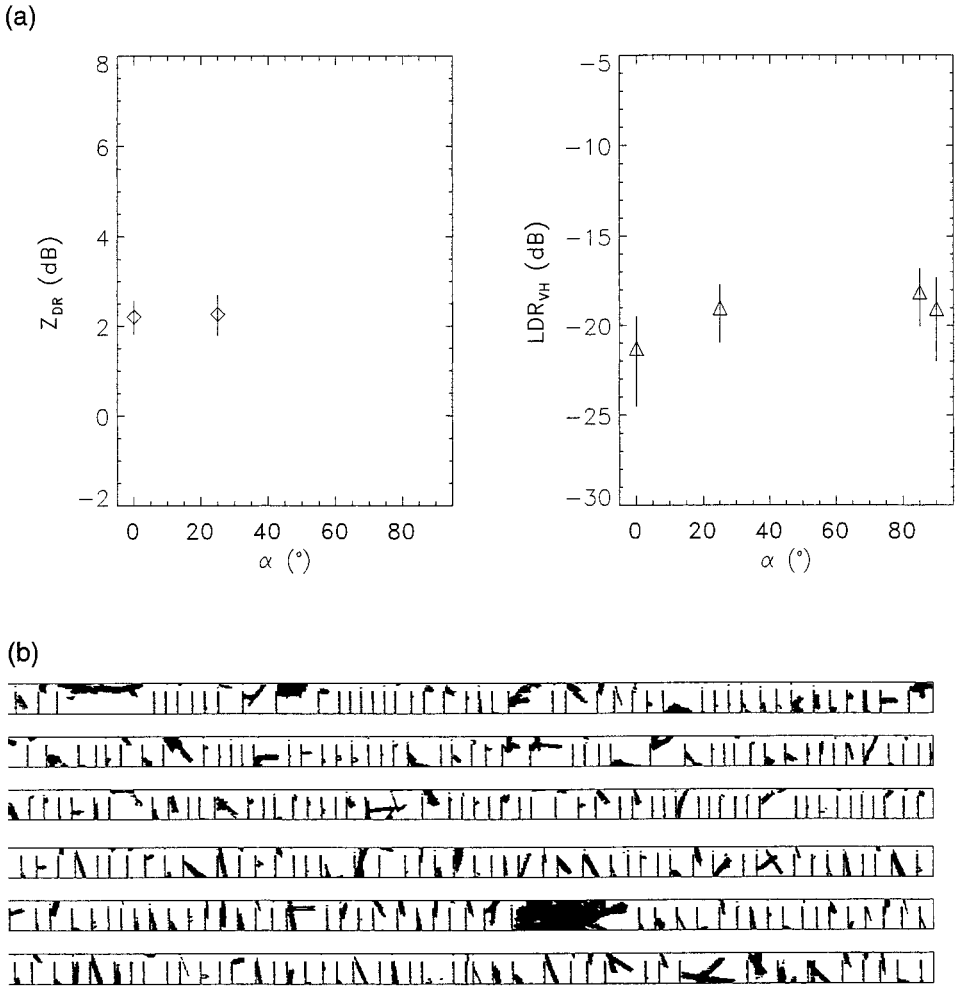

FIG. 3. (a) Same as Fig. 1 except for lightly rimed needle crystals (R1a) listed in lines 10–11 and 26–27 of Table 1. (b) Sample 2D-C images with 800-μm-wide image strips.

at high α; it increases from near -16 dB at $\alpha \approx 15°$ to -13 dB at $\alpha > 60°$.

e. High LDR observation with graupel

On two different occasions (Table 1, lines 20–21 and 35–36), unexpectedly high values of LDR were observed in cumulus congestus. In both cases, the high LDR values were observed in cloud volumes consisting of graupel with sizes of 4–6 mm mixed with other small hydrometeors. The temperature and liquid water contents for both situations rule out ''wet growth'' of the graupel. Lighting activity was noted in both cases, but the in situ data show no needle crystals, which might have been aligned by electric fields. Thus, the high LDR observations remain unexplained. Until better identification is obtained, we will refer to these situations as ''special graupel'' cases.

Figure 5 shows the mean and standard deviations of Z_{DR} and LDR_{HV} versus α in regions of the high-LDR zones of 4 April 1997, sample 2D-P images and the size distribution of hydrometeors for one data segment. As can be seen from the hydrometeor spectrum and the 2D-P images, the high LDR regions correspond to regions of high concentrations of small hydrometeors mixed with large (3–6 mm) graupel. Negative Z_{DR} values (-1.0 to -0.5 dB) were recorded in the high-LDR zone, particularly for low elevation angles ($\alpha < 20°$). The mean LDR_{HV} decreased from near -7 dB at $\alpha < 5°$ to -15 dB at α range of 55°–60° and increased slightly for α between 60° and 90°. Reinking et al. (1997b) also reported some orientation effects for graupel. They measured (at 35 GHz) LDR values of -30 to -32 dB at vertical beam orientation. This value is much lower than our measurements.

6. Summary of polarimetric signatures

Results obtained for different crystal types are summarized in Fig. 6 as domains of Z_{DR} and LDR for near-horizontal and for near-vertical beam orientations. The indicated domains correspond to the ranges of values

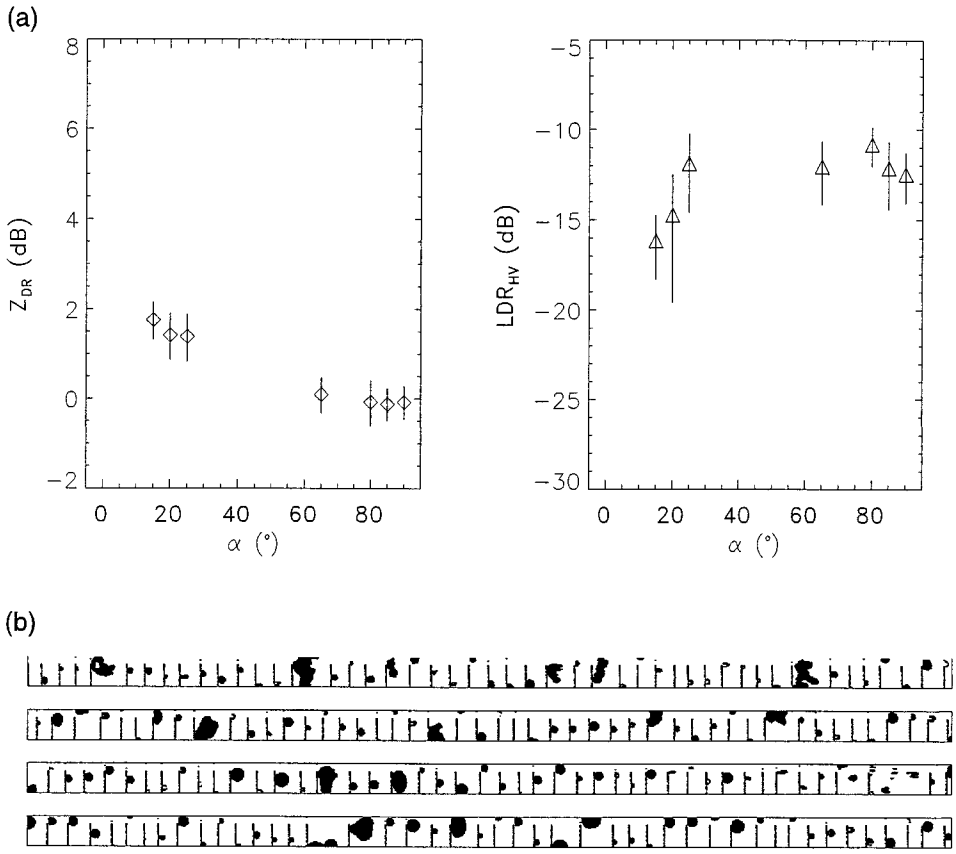

FIG. 4. (a) Same as Fig. 1, except for observations taken within the melting layer, as listed in lines 18–19 and 33–34 of Table 1. (b) Sample 2D-C images with 800-μm-wide image strips.

given in Table 1. The −22-dB break on the LDR axis in the figure represent the cross-polarized detection limit of the WCR; only Z_{DR} can be used to characterize crystal types from our data below that value of LDR.

Of the pristine crystal types observed in the WYICE97 dataset, planar P1a and P1d crystals produced the highest Z_{DR} values, up to 8 dB, for near-horizontal incidence. This provides the main distinguishing feature for these crystals. It appears that the reduced density of the branched P1d crystals, in comparison with the basic hexagonal plate form of the P1a crystals, does not significantly affect the polarimetric signatures, most likely because of a compensating difference in the aspect ratios of the crystals, since aspect ratio generally increases with size. These results agree with the modeling results of AT97. Not included as a parameter in Fig. 6, but demonstrated with the data in lines 1–3 in Table 1, there is a clear dependence of the magnitudes of Z_{DR} and LDR on crystal size. This too may be an indirect effect of changes in aspect ratios with size.

The Z_{DR} values for P1e (dendritic) crystals are lower than for P1a and P1d crystals by about 3–5 dB at near-horizontal incidence. On the other hand, LDR_{HV} values for P1e crystals are either comparable or higher than for P1a and P1d crystals. The higher LDR and lower Z_{DR} for near-horizontal beam conflict with the nearly identical model results for these two crystal types reported by Reinking et al. (1997a). One possible interpretation of our measurements is a larger range of canting angles with the P1e crystals than assumed in the calculations. Vivekanandan et al. (1994) reported Z_{DR} values of up to 4 dB for dendritic crystals.

The ranges of Z_{DR} and LDR values for columnar crystals are quite different from those for planar crystals. For low α, the Z_{DR} values from needles are lower than the values observed in P1a and P1d crystals but comparable to or higher than for P1e crystals. LDR changes with α in the opposite way to what is observed for planar crystals. This increase of LDR with α agrees with the findings of Reinking et al. (1997a), AT97, Evans et al. (1990), and others who indicated that planar crystals could be distinguished from columnar crystals based on the LDR trend with α.

In the melting layer, Z_{DR} values for near-horizontal incidence angles are comparable with values observed for columnar and P1e crystals. However, melting crystals produce much higher LDR values than columns. Also, since the LDR values for P1e crystals for near-vertical beam are much lower than the values observed from the melting crystals, there is a basis for differ-

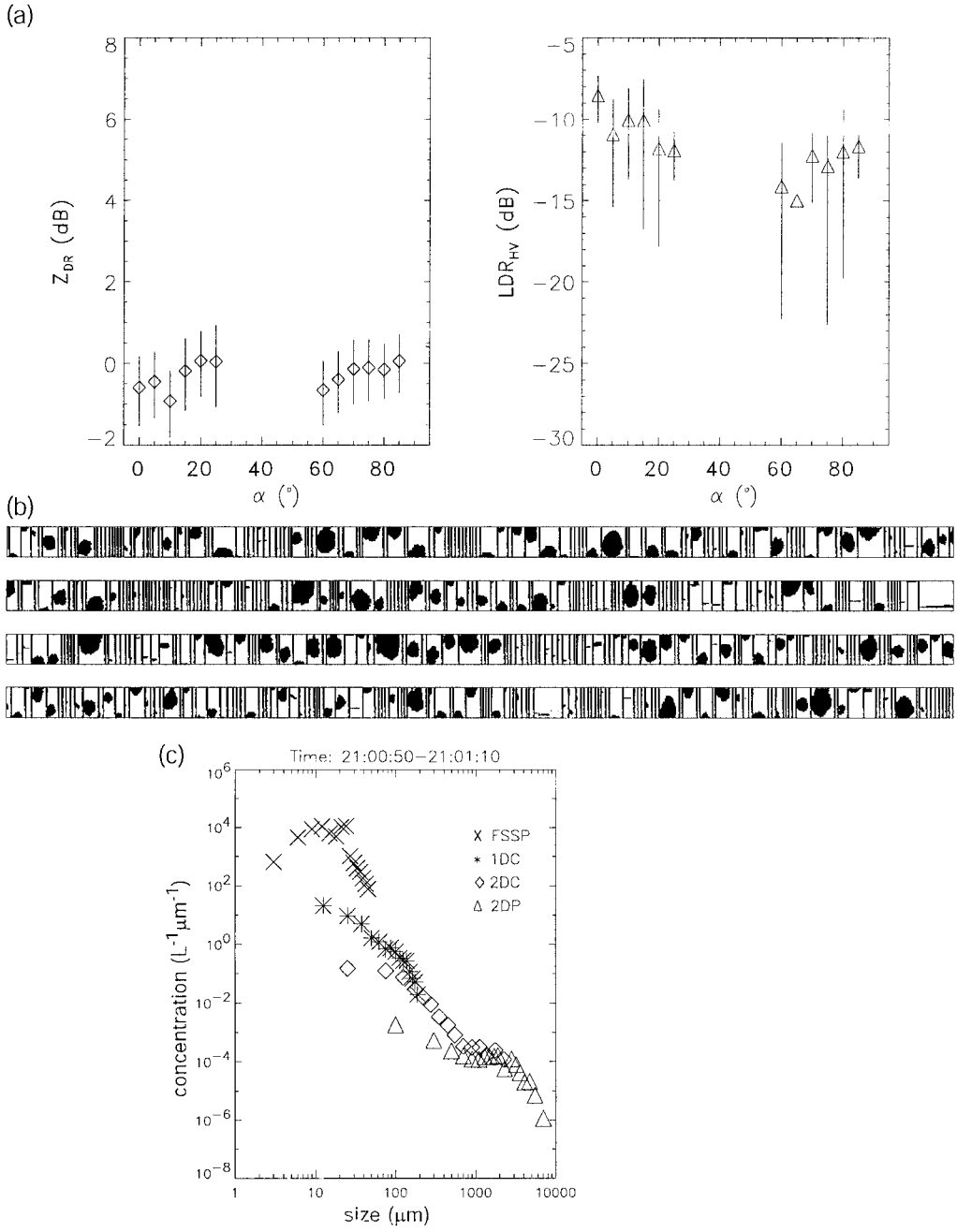

FIG. 5. (a) Same as Fig. 1 except for special graupel situations listed in lines 20–21 and 35–36 of Table 1. (b) Sample 2D-P images with 6.4-mm-wide image strips. (c) Size distribution for data segment of line 21, Table 1.

entiating melting crystals from both columnar and P1e crystals. Similar to columnar crystals, LDR in the melting layer increases with an increased incidence angle, but the LDR in the melting layer is at least 5 dB higher than for columnar crystals at near-horizontal incidence.

The Z_{DR} and LDR_{HV} signatures we observed in the ''special graupel'' cases are unique in comparison with the other crystal types. For near-horizontal incidence, Z_{DR} values are near zero, which can also be found for densely rimed crystals, large aggregates, and drizzle drops. On the other hand, LDR_{HV} values for low α are higher than observed for any ice crystal type, including the melting layer. For high α, however, LDR_{HV} values are comparable to those from the melting layer. At least for these special graupel cases, the LDR trend with α is opposite to that for the melting layer.

Some qualitative inferences can also be drawn from the Z_{DR} and LDR observations regarding crystal ori-

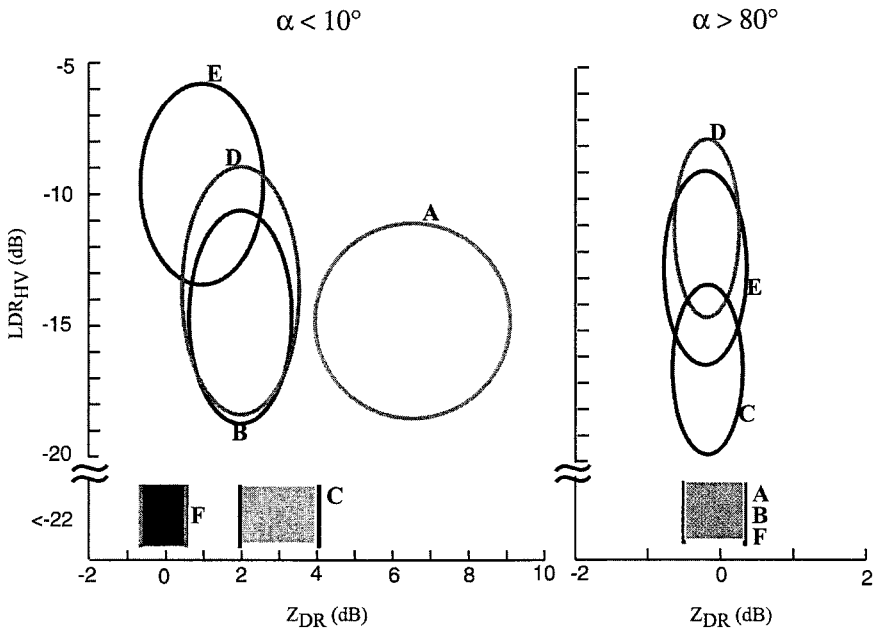

FIG. 6. Summary of observations reported in this paper in terms of typical Z_{DR} and LDR_{HV} signatures of different ice crystal types for near-horizontal (left-hand panel) and near-vertical (right-hand panel) radar elevation angles. LDR < -22 dB represents the detection limit achieved.

entations. For all crystal types considered in this study, the maximum Z_{DR} values are observed for beam incidence angles near 0°. These observations indicate that the mean canting angles are near 0° for platelike crystals and 90° for columnar shapes. In addition, $Z_{DR} \approx 0$ dB for near-vertical incidence indicates random orientations of the crystals in the horizontal plane.

The degree of variation of crystal orientation about the mean, characterized by the standard deviation of canting angles, changes with crystal type. For P1a/P1d crystals the deviations are small; comparison of the observed Z_{DR} values with the result of AT97 suggest $\sigma_\theta < 20°$. For P1e types, the observations of high LDR with low Z_{DR} for near-horizontal incidence suggest high canting angle standard deviation.

7. Conclusions

As shown in Fig. 6, there is a reasonable basis for distinguishing crystals of various growth habits based on the two polarimetric measures here employed and on the variation of these measures with the incidence angle of the radar beam. With the exceptions of the melting band and the special graupel cases, polarimetric signatures are associated with unrimed or slightly rimed crystals and are thus identifiers of cloud regions where such crystals exist. Since growth by deposition is the first stage of crystal growth, the radar signatures are helpful in identifying cloud regions that may be still relatively close to the regions of crystal origin. However, in vigorous clouds of high liquid water contents such regions will be small and short-lived, and thus difficult to detect. At the other extreme, in layer clouds with little or no liquid water content crystals remain unrimed throughout the cloud volume so the absence of riming is not indicative of recent crystal origins. A third limitation arises from inadequate radar sensitivity, which currently permits the detection of crystals only after they have reached several hundred micrometers in size, though this limit also depends on the concentration of crystals.

Identification of specific crystal habits is perhaps of lesser practical importance than the distinction between pristine and rimed crystals. This is because the growth habits of crystals are, in general, well predicted by temperature. Our data revealed no surprises in this regard. It is conceivable that further improvements in the acuity of classification by radar may lead to some insights into atmospheric processes not yet appreciated, but currently that prospect appears remote.

Of the two exceptions mentioned above, where polarimetric signatures are not associated with unrimed crystals, the melting band is not a serious concern for misinterpretation of polarimetric signatures as its location is usually well known. The special graupel cases, if data are available at both horizontal and vertical incidence angles, are distinguishable from pristine crystals. But, these graupel observations are of interest because of the strong orientation effects implied by the LDR values. So far, since we have seen such occurrences in few cases only and in quite limited cloud regions, we have no plausible explanations for them. It is possible that small crystals that are not well detected by the in situ probes were actually responsible for the polarization signatures. This possibility is worth exploring, as it may turn out to be evidence for situations of secondary ice production.

The results shown in Fig. 6 are based on nearly coincident observations of crystal type and radar backscatter, and are therefore an improvement over earlier studies in which the remotely sensed data and the cloud particle data were not as tightly coupled. However, since size distributions, shapes, and the degree of oscillations of the crystals can vary beyond the ranges covered in our samples, the generality of these results will have to be established with further observations. Also, if LDR values lower than our −22-dB limit could be reliably detected, the diagnoses of crystal type might be further improved. It should also be noted that our data did not include samples of large aggregates of dendritic or needle crystals; these additions are needed to complete Fig. 6.

Our results derived from 95-GHz airborne radar complement the results obtained by the National Oceanic and Atmospheric Administration Environmental Technology Laboratory group with a 35-GHz ground-based radar (see references by Matrosov, Reinking, and colleagues). Their radar has greater sensitivity; the airborne radar has the capability to achieve proximity to cloud regions of interest. There are many parallels between their and our measurements and some numerical comparisons have been already mentioned. Qualitative trends with elevation angle are also the same in the two sets of measurements. More extensive comparisons are not possible, as the majority of their results are for elliptical polarization, not linear, and for elevation angles of 45° and 90°. Theory predicts somewhat higher depolarization ratios for higher-frequency radars, so the potential exists to explore this difference with simultaneous observations, though the precision needed in the measurements and the homogeneity that would have to exist in the cloud are unlikely to be realized.

Unavoidably, uniformity over an appreciable cloud volume is required to allow observations at several incidence angles using a single radar unit. With the airborne system and rapid switching of beam orientation, uniformity over a few hundreds of meters is needed to provide meaningful analyses; for the ground-based observations of Reinking et al. (1997a) the required scale was 10–20 km.

Melting crystals can also be identified based on their polarimetric signatures, though knowledge of the height of the 0°C level in the atmosphere usually makes this diagnosis easy anyway. The vertical depth of the melting layer as seen in the reflectivity and polarization fields contains additional information on the type and size of the hydrometeors, as do the polarization parameters just above the melting layer. However, interpretation of the radar observations in melting layers in terms of hydrometeor shape, size, and density is still quite uncertain.

Comparisons of the observations with model calculations are generally favorable, at least in trends and in relative values from one crystal type to another. Absolute values of the observed polarization parameters cannot be reliably compared with published calculations because of differences between the assumed and observed size distributions, canting angles, etc. Direct comparisons may be possible in the future. A few definite puzzles also emerged, such as the high LDR values for dendritic crystals at horizontal beam orientation, and the large values of LDR observed for the special graupel case at both horizontal and vertical incidence angles.

Acknowledgments. Many people have participated in the data collection and processing. Dr. R. D. Kelly is co-principal investigator of the project and has contributed generously to all aspects of this study. He, D. Leon, and Drs. J. French and S. Haimov have participated in the field experiment and in the data processing. The work of the University of Wyoming King Air Flight Facility was indispensable for the success of the experiment. K. Endsley, P. Wechsler, G. Gordon, the pilots, and technicians supporting the King Air have done an outstanding job in the field work and data processing. We also wish to thank Drs. A. L. Pazmany and the late R. E. McIntosh from the Microwave Remote Sensing Laboratory, University of Massachusetts at Amherst, for their unstinting efforts to make this work possible. We would like to also thank Drs. Kultegin Aydin and Thomas Walsh for providing their FDTD parametric fits and useful discussion related to this work. This work was supported by National Science Foundation Grants ATM-9319907 and ATM-9712859. The 1995 coastal stratus study, from which some data were also used, was supported by a DEPSCOR grant from the Office of Naval Research. We appreciate the care taken by two reviewers in improving the manuscript.

REFERENCES

Aydin, K., and C. Tang, 1997: Millimeter wave radar scattering from model ice crystal distributions. *IEEE Trans. Geosci. Remote Sens.*, **35,** 140–146.

——, and T. Walsh, 1999: Millimeter wave scattering from spatial and planar bullet rosettes. *IEEE Trans. Geosci. Remote Sens.*, **37,** 1138–1150.

——, T. A. Seliga, and V. N. Bringi, 1984: Differential radar scattering

properties of model hail and mixed hydrometeors. *Radio Sci.,* **19,** 58–66.

——, C. Tang, A. Pazmany, J. Mead, R. McIntosh, M. Hervig, R. Kelly, and G. Vali, 1994: 95 GHz polarimetric radar measurements in a cloud compared with model computations. *Atmos. Res.*, **34,** 135–144.

Bader, M. J., S. A. Clough, and G. P. Cox, 1987: Aircraft and dual polarization radar observations of hydrometeors in light stratiform precipitation. *Quart. J. Roy. Meteor. Soc.*, **113,** 491–515.

Bringi, V. N., L. Liu, P. C. Kennedy, V. Chandrasekar, and S. A. Rutledge, 1996: Dual multiparameter radar observations of intense convective storms: The 24 June 992 case study. *Meteor. Atmos. Phys.*, **59,** 3–31.

Cox, D. C., H. W. Arnold, and H. H. Hoffman, 1978: Depolarization of 19 and 28 GHz earth–space signals by ice particles. *Radio Sci.,* **13,** 511–517.

Doviak, R. J., and D. S. Zrnić, 1993: *Doppler Radar and Weather Observations.* Academic Press, 562 pp.

Evans, K., and J. Vivekanandan, 1990: Multiparameter radar and microwave radiative transfer modeling of nonspherical atmospheric ice particles. *IEEE Trans. Geosci. Remote Sens.,* **28,** 423–437.

Fabry, F., and W. Szyrmer, 1999: Modeling of the melting layer. Part II: Electromagnetics. *J. Atmos. Sci.,* **56,** 3593–3600.

Galloway, J., A. Pazmany, J. Mead, R. McIntosh, D. Leon, J. French, R. Kelly, and G. Vali, 1997: Detection of ice hydrometeor alignment using an airborne W-Band polarimetric radar. *J. Atmos. Oceanic Technol.,* **14,** 3–12.

Hakkarinen, I. M., and R. F. Adler, 1988: Observations of precipitating convective systems at 92 and 183 GHz: Aircraft results. *Meteor. Atmos. Phys.*, **38,** 164–182.

Hall, M. P. M., W. F. Goddard, and S. M. Cherry, 1984: Identification of hydrometeors and other targets by dual-polarization radar. *Radio Sci.,* **19,** 132–140.

Herzegh, P., and A. R. Jameson, 1992: Observing precipitation through dual-polarization radar measurements. *Bull. Amer. Meteor. Soc.,* **73,** 1365–1374.

Intrieri, J. M., G. L. Stephens, W. L. Eberhard, and T. Uttal, 1993: A method for determining cirrus cloud particle sizes using lidar and radar backscatter technique. *J. Appl. Meteor.,* **32,** 1074–1082.

Jameson, A. R., and D. Johnson, 1990: Cloud microphysics and radar. *Radar in Meteorology,* D. Atlas, Ed., Amer. Meteor. Soc., 323–340.

Lohmeier, S. P., S. M. Sekelsky, J. M. Firda, G. A. Sadowy, and R. E. McIntosh, 1997: Classification of particles in stratiform clouds using the 33 and 95 GHz polarimetric cloud profiling radar system (CPRS). *IEEE Trans. Geosci. Remote Sens.*, **35,** 256–270.

Magono, C., and C. W. Lee, 1966: Meteorological classification of natural snow crystals. *J. Fac. Sci. Hokkaido Univ. Ser. VII,* **2,** 321–362.

Matrosov, S. Y., 1991a: Prospects for the measurement of ice cloud particle shape and orientation with elliptically polarized radar signals. *Radio Sci.,* **26,** 847–856.

——, 1991b: Theoretical study of radar polarization parameters obtained from cirrus clouds. *J. Atmos. Sci.,* **48,** 1062–1070.

——, 1997: Variability of microphysical parameters in high-altitude ice clouds: Results of the remote sensing method. *J. Appl. Meteor.,* **36,** 633–648.

——, and R. A. Kropfli, 1993: Cirrus cloud studies with elliptically polarized Ka-band radar signals: A suggested approach. *J. Atmos. Oceanic Technol.,* **10,** 684–692.

——, T. Uttal, J. B. Snider, and R. A. Kropfli, 1992: Estimation of ice cloud parameters from ground-based infrared radiometer and radar measurements. *J. Geophys. Res.,* **97,** 11 567–11 574.

——, R. F. Reinking, R. A. Kropfli, and B. W. Bartram, 1996: Estimation of ice hydrometeor types and shapes from radar polarization measurements. *J. Atmos. Oceanic Technol.,* **13,** 85–96.

McCormick, G. C., and A. Hendry, 1975: Principles for the radar determination of the polarization properties of precipitation. *Radio Sci.,* **10,** 421–434.

Pasqualucci, F., B. W. Bartram, R. A. Kropfli, and W. R. Moninger, 1983: A millimeter-wavelength dual-polarization Doppler radar for cloud and precipitation studies. *J. Climate Appl. Meteor.,* **22,** 758–765.

Pazmany, A. L., R. E. McIntosh, R. D. Kelly, and G. Vali, 1994a: An airborne 95 GHz dual-polarized radar for cloud studies. *IEEE Trans. Geosci. Remote Sens.,* **32,** 731–739.

——, ——, J. Mead, R. McIntosh, M. Hervig, R. Kelly, and G. Vali, 1994b: 95-GHz polarimetric radar measurements of orographic cap clouds. *J. Atmos. Oceanic Technol.,* **11,** 140–153.

Politovich, M. K., B. B. Stankov, and B. E. Martner, 1995: Determination of liquid water altitudes using combined remote sensors. *J. Appl. Meteor.,* **34,** 2060–2075.

Reinking, R. F., S. Y. Matrosov, R. T. Bruintjes, and B. E. Martner, 1997a: Identification of hydrometeors with elliptical and linear polarization K_a- band radar. *J. Appl. Meteor.,* **36,** 322–339.

——, ——, B. E. Martner, and R. A. Kropfli, 1997b: Dual-polarization radar to identify drizzle, with applications to aircraft icing avoidance. *J. Aircraft,* **34,** 778–784.

Sekelsky, S. M., and R. E. McIntosh, 1996: Cloud observations with a polarimetric 33 GHz and 95 GHz radar. *Meteor. Atmos. Phys.,* **59,** 123–140.

——, W. L. Ecklund, J. M. Firda, K. S. Gage, and R. E. McIntosh, 1999: Particle size estimation in ice clouds using multifrequency radar reflectivity measurements at 95, 33, and 2.8 GHz. *J. Appl. Meteor.*, **38,** 5–28.

Seliga, T. A., and V. N. Bringi, 1976: Potential use of radar differential reflectivity measurements at orthogonal polarizations for measuring precipitation. *J. Appl. Meteor.,* **15,** 69–75.

Stankov, B. B., B. E. Martner, and M. K. Politovich, 1995: Moisture profiling of the cloudy winter atmosphere using combined remote sensors. *J. Atmos. Oceanic Technol.,* **12,** 488–510.

Szyrmer, W., and I. Zawadzki, 1999: Modeling of the melting layer. Part I: Dynamics and microphysics. *J. Atmos. Sci.,* **56,** 3573–3592.

Vivekanandan, J., V. N. Bringi, M. Hagen, and P. Meischner, 1994: Polarimetric radar studies of atmospheric ice particles. *IEEE Trans. Geosci. Remote Sens.,* **32,** 1–10.

Wolde, M., and G. Vali, 2001: Polarimetric signatures from ice crystals observed at 95 GHz in winter clouds. Part II: Frequencies of occurrence. *J. Atmos. Sci.,* **58,** 842–849.